Production of a prompt photon in association with a charm quark at next-to-leading order in QCD

B. Bailey
Physics Department, Eckerd College, St. Petersburg, Florida 33711

Edmond L. Berger and L. E. Gordon
High Energy Physics Division, Argonne National Laboratory, Argonne, Illinois 60439

(Received 23 February 1996)

A second order $O(\alpha_s^2)$ calculation in perturbative quantum chromodynamics of the two particle inclusive cross section is presented for the reaction $p+\overline{p}\rightarrow\gamma+c+X$ for large values of the transverse momentum of the prompt photon and charm quark. The combination of analytic and Monte Carlo integration methods used here to perform phase-space integrations facilitates the imposition of photon isolation restrictions and other selections of relevance in experiments. Differential distributions are provided for various observables. Positive correlations in rapidity are predicted. [S0556-2821(96)04415-3]

PACS number(s): 12.38.Bx, 12.38.Qk, 13.85.Ni, 13.85.Qk

I. INTRODUCTION

More precise examination of the expectations of perturbative quantum chromodynamics (QCD), including dynamical correlations inherent in the hard-scattering matrix elements, is made possible by the observation of inclusive production of two particles or jets, each carrying a large value of transverse momentum. Because they couple in a pointlike fashion to quarks, the observation of photons with large values of transverse momentum in a high energy hadron collision has long been regarded as an incisive probe of short-distance dynamics. In the case of inclusive production of heavy quarks, the large mass of the quark and/or the fact that the quark carries large transverse momentum justifies use of a perturbative short-distance approach. In this paper, we continue our examination of the associated production of a prompt photon along with a heavy quark [1]. Data are beginning to become available on the associated production of a photon γ carrying large transverse momentum along with a charm quark c whose transverse momentum balances a substantial portion of that of the photon [2]. An intriguing possibility is that the data may be used to measure the charm quark density in the nucleon.

In this paper we report results of a full next-to-leading order perturbative QCD calculation of $p+\overline{p}\rightarrow\gamma+c+X$ at high energy. For values of the transverse momentum p_T^c of the charm quark much larger than the mass m_c of the quark, only one *direct* hard-scattering subprocess contributes in leading order: the quark-gluon Compton subprocess $gc\rightarrow\gamma c$. The initial charm quark and the initial gluon are constituents of the initial hadrons. In addition, there is a leading order *fragmentation* process in which the photon is produced from quark or gluon fragmentation, e.g., $gg\rightarrow c\overline{c}$ followed by $\overline{c}\rightarrow\gamma X$ or $qc\rightarrow qc$ followed by $q\rightarrow\gamma$. At next-to-leading order in QCD, several subprocesses contribute to the $\gamma+c+X$ final state: $gc\rightarrow gc\gamma$, $gg\rightarrow c\overline{c}\gamma$, $q\overline{q}\rightarrow c\overline{c}\gamma$, $qc\rightarrow qc\gamma$, $q\overline{c}\rightarrow q\overline{c}\gamma$, $c\overline{c}\rightarrow c\overline{c}\gamma$, and $cc\rightarrow cc\gamma$. A full next-to-leading order calculation requires the computation of the hard-scattering matrix elements for these two-to-three particle production processes as well as the one-loop $O(\alpha_s^2)$ corrections to the lowest order subprocess $gc\rightarrow\gamma c$.

We are interested ultimately in the fully differential two-particle inclusive cross section $E_\gamma E_c d\sigma/d^3p_\gamma d^3p_c$, where (E,p) represents the four-vector momentum of the γ or c quark. For each contributing subprocess, this calculation requires integration over the momentum of the unobserved final parton in the two-to-three particle subprocesses (g, $\overline{c}$, q, or $\overline{q}$). Collinear singularities must be handled analytically by dimensional regularization and absorbed into parton momentum densities or fragmentation functions. In the theoretical analysis reported here, a combination of analytic and Monte Carlo integration methods is used to perform phase-space integrations over unobserved final-state partons and the momenta of the initial partons. This approach facilitates imposition of photon isolation restrictions and other selections of relevance in experiments. We work in the massless approximation $m_c=0$. To warrant use of perturbation theory and the massless approximation, we limit our considerations to values of transverse momenta of the photon and charm quark of $p_T^{\gamma,c}>10$ GeV.

In the lowest order direct subprocess, $gc\rightarrow\gamma c$, the prompt photon emerges in isolation from the only other particle in the hard scattering, the charm quark. Long-distance quark-to-photon and gluon-to-photon fragmentation processes have been emphasized theoretically [3] and parametrized phenomenologically in leading order [4], and evolved in next-to-leading order [5,6]. These terms may account for more than half of the calculated inclusive single-photon cross section at modest values of transverse momentum at the Fermilab Tevatron collider. Photons originating through fragmentation are likely to emerge in the neighborhood of associated hadrons. An experimental isolation restriction is needed before a clean identification can be made of the photon and a measurement made of its momentum. Isolation reduces the size of the observed fragmentation contribution. Photon isolation complicates the theoretical interpretation of results, however, since it threatens to upset the cancellation of infrared divergences in perturbation theory [7]. In this

 © 1996 The American Physical Society

paper, we include the fragmentation contributions, and we impose isolation requirements through our Monte Carlo method.

A combination of analytic and Monte Carlo methods similar to that we employ in this paper has been used to carry out next-to-leading order QCD calculations of other processes including inclusive prompt photon [8] and photon pair [9] production in hadron collisions, and single [10] and pair production of heavy gauge bosons [11]. Prompt photon plus associated charm production at large values of transverse momentum has also been addressed in Ref. [12], but our analysis differs from theirs. The calculation in Ref. [12] is done in lowest order while ours is done at next-to-leading order. In lowest order, the subprocesses $gg\to\gamma c\overline{c}$ and $q\overline{q}\to\gamma c\overline{c}$ contribute in the massive case, whereas $cg\to\gamma c$ plus fragmentation processes contribute in the massless case. In a forthcoming paper, we intend to examine the massive case in detail and to discuss comparisons with the massless case in the regions of phase space of their respective applicability. As remarked above, our massless approach should be appropriate and applicable in the domain in which there is effectively only one large scale, $p_T^c \gg m_c$.

In Sec. II, we describe the combination of analytic and Monte Carlo methods we use to carry out the next-to-leading order calculation. The next-to-leading order calculation itself is presented in Sec. III. Differential cross sections and other numerical results are discussed in Sec. IV. Summary remarks are collected in Sec. V. An appendix is included in which we derive analytic expressions for some of the parton level cross sections we use.

II. MONTE CARLO METHOD

The combination of analytic and Monte Carlo techniques used here to perform the phase-space integrals is documented and described in detail elsewhere [8–11], and so our discussion will be fairly brief, highlighting features important to our calculation. For the two-to-three particle hard-scattering subprocesses, the technique consists in identifying those regions of phase space where soft and collinear singularities occur and integrating over them analytically in $4-2\epsilon$ dimensions. In this way the singularities are exposed as poles in ϵ. These regions are isolated from the rest of the three-body phase space by the imposition of arbitrary boundaries through the introduction of cutoff parameters δ_s and δ_c. The soft-gluon region of phase space is defined to be the region in which the gluon energy, in a specified reference frame, usually the subprocess rest frame, falls below a certain threshold $\delta_s\sqrt{\hat{s}}/2$, where δ_s is the cutoff parameter and $\hat{s}$ is the center-of-mass energy in the initial parton-parton system. Labeling the momenta for the general three-body process by $p_1+p_2\to p_3+p_4+p_5$, we define the general invariants by $s_{ij}=(p_i+p_j)^2$ and $t_{ij}=(p_i-p_j)^2$. The collinear region is defined as the region in which the value of an invariant falls below the value $\delta_c\hat{s}$.

The full set of three-body final-state subprocesses is

$$g+c\to g+c+\gamma, \tag{2.1a}$$

$$g+g\to c+\overline{c}+\gamma, \tag{2.1b}$$

$$q+\overline{q}\to c+\overline{c}+\gamma, \tag{2.1c}$$

$$q+c\to q+c+\gamma, \tag{2.1d}$$

$$\overline{q}+c\to\overline{q}+c+\gamma, \tag{2.1e}$$

$$c+\overline{c}\to c+\overline{c}+\gamma, \tag{2.1f}$$

$$c+c\to c+c+\gamma. \tag{2.1g}$$

The matrix elements integrated over the mutually exclusive soft and collinear regions of phase space are not the full two-to-three body matrix elements but, instead, specific approximate versions. In the soft-gluon case the approximate version is obtained by setting the gluon energy to zero everywhere it occurs in the matrix elements, except in the denominators. For the collinear singularities, each invariant that vanishes is in turn set to zero everywhere except in the denominator. This form is the leading pole approximation. The phase-space integrals are performed with these approximate expressions, and only the terms proportional to logarithms of the cutoff parameters are retained. Terms proportional to positive powers of the cutoff parameters are set to zero. In order for the method to yield reliable results, the cutoff parameters must be kept small; otherwise, the approximations would not be valid.

After the two-to-three particle phase space integrals are performed analytically over the singular regions and the soft and collinear poles are exposed, the $O(\alpha_s^2)$ virtual gluon-exchange loop contributions, if any, are added, and all double poles and single poles of soft (infrared) origin are verified to cancel, as they should. The remaining collinear singularities are factored into parton distribution and fragmentation functions at an appropriate factorization or fragmentation scale. We work in the modified minimal subtraction ($\overline{\rm MS}$) scheme. One is left with a set of matrix elements for effective two-body final-state processes that depend explicitly on $\ln\delta_s$ and $\ln\delta_c$. In addition, the nonsingular regions of phase space yield a set of three-body final-state matrix elements which, when integrated over phase space by Monte Carlo techniques, have an implicit dependence on these same logarithms. The signs are such that the dependences on $\ln\delta_s$ and $\ln\delta_c$ cancel between the two-body and three-body contributions. The physical cross sections are independent of these arbitrary cutoff parameters over wide ranges. In our numerical work, we varied δ_s and δ_c over suitable ranges and found quite stable results, as is shown in Sec. IV.

At the level of two-body final-state matrix elements, as in leading-order calculations, it is a simple matter to impose selections on kinematic variables similar to those made in experiments and to calculate different observables. The same is not the case when we consider three-body final-state processes. The standard analytic techniques required to obtain differential cross sections of empirical interest often involve complex Jacobian transformations, and the phase-space integrals can sometimes be done analytically only when specific limits of integration are involved. Fully analytic methods of performing calculations for physical processes, although in some cases desirable, can be rather restricted in their usefulness when it is desirable and sometimes even unavoidable that kinematic selections be made to model experimental

cuts. The combined analytic and Monte Carlo method is particularly versatile in that it provides a means to calculate cross sections differential in many variables at once and to apply cuts on the kinematic variables to match those made in the experiments. The phase-space integrals are performed numerically after all singularities have been handled analytically.

Our calculation of photon plus charm quark production proceeds along lines similar to that for inclusive direct photon production described in Ref. [8], but with a few important differences. Since we are interested in observing a final charm quark as well as the photon, we cannot integrate analytically over phase space in the limit in which the charm quark is collinear to a hard gluon or a charm antiquark. This situation occurs in the cg-, $c\overline{c}$-, and $q\overline{q}$-initiated processes of Eq. (2.1). The expression in the appendix of Ref. [8] for the sum of all effective two-body contributions cannot be used in our calculation. We recalculated this expression using the three-body matrix elements and virtual gluon-exchange contributions from Ref. [13], and we provide the results in the Appendix. We also discuss and present in the Appendix the final-state collinear remnants that give the charm quark momentum distribution in the limit that the charm quark is produced collinearly with an anticharm quark or a gluon. The singularities in these cases are factored into charm quark fragmentation functions.

III. CONTRIBUTIONS THROUGH NEXT-TO-LEADING ORDER

A. Leading-order contributions

In leading order in perturbative QCD, only one *direct* subprocess contributes to the hard-scattering cross section, the QCD Compton process $cg\rightarrow\gamma c$, unlike the case for single inclusive prompt photon production, where the annihilation process $q\overline{q}\rightarrow\gamma g$ also contributes. Since the leading-order direct partonic subprocess has a two-body final state, the photon and c quark are produced with balancing transverse momenta. In addition, there are effectively leading-order contributions in which the photon is produced by fragmentation from a final-state parton. These are

$$\begin{aligned} &c+g\rightarrow g+c,\\ &g+g\rightarrow c+\overline{c},\\ &c+q\rightarrow c+q,\\ &c+\overline{q}\rightarrow c+\overline{q},\\ &c+c\rightarrow c+c,\\ &c+\overline{c}\rightarrow c+\overline{c},\\ &q+\overline{q}\rightarrow c+\overline{c}. \end{aligned} \tag{3.1}$$

If the photon is to be isolated from the observed charm quark, it arises from fragmentation of the gluon g and the noncharm quark q, respectively, in the cases of the first, third, and fourth processes. In the other cases it is produced by fragmentation of one of the (anti)charm quarks.

In a fully consistent next-to-leading calculation, one should calculate the subprocesses in Eq. (3.1) to $O(\alpha_s^3)$, since the photon fragmentation functions that are convoluted with the hard subprocess cross sections are of $O(\alpha_{\rm em}/\alpha_s)$. For simplicity, we include them in $O(\alpha_s^2)$ only. In fact, next-to-leading order fragmentation contributions to single prompt photon production have been included only once before [13]. We expect the next-to-leading order corrections to the fragmentation contributions to be insignificant numerically especially after isolation cuts are imposed.

B. Next-to-leading order contributions

There are two classes of contributions in next-to-leading order. First there are the virtual gluon-exchange corrections to the lowest order process, $cg\rightarrow\gamma c$. Examples are shown in Fig. 1(b). These amplitudes interfere with the Born amplitudes and contribute at $O(\alpha_{\rm em}\alpha_s^2)$. They were calculated twice before [8,13]. At next-to-leading order there are also three-body final-state contributions, listed in Eq. (2.1). The matrix elements for these are also taken from Ref. [13], where they are calculated for single inclusive prompt photon production.

The main task of our calculation is to integrate the three-body matrix elements over the phase space of the unobserved particle in the final state. The situation here is different from the standard case of single inclusive particle production because we wish to retain as much control as possible over the kinematic variables of a second particle in the final state, while at the same time integrating over enough of the phase space to ensure cancellation of all infrared and collinear divergences, inherent when massless particles are assumed. All the processes of Eq. (2.1), except the first, involve collinear singularities but no soft singularities. These collinear singularities must be exposed and factored as explained in Sec. II. The results of these calculations are listed in the Appendix.

At $O(\alpha_s^2)$ there are, in addition, fragmentation processes in which the hard-scattering two-particle final-state subprocesses

$$\begin{aligned} &c+g\rightarrow\gamma+c,\\ &c+\overline{c}\rightarrow\gamma+g,\\ &q+\overline{q}\rightarrow\gamma+g \end{aligned} \tag{3.2}$$

are followed by fragmentation processes $c\rightarrow cX$, in the case of the first subprocess, and $g\rightarrow cX$ in the cases of the last two. These should be included because we have factored the collinear singularities in the corresponding three-body final-state processes into nonperturbative fragmentation functions for production of a charm quark from a particular parton. As a first approximation, we estimate these fragmentation functions by

$$D_{c/c}(z,\mu^2)=\frac{\alpha_s(\mu^2)}{2\pi}P_{qq}(z) \tag{3.3}$$

and

$$D_{c/g}(z,\mu^2)=\frac{\alpha_s(\mu^2)}{2\pi}P_{qg}(z), \tag{3.4}$$

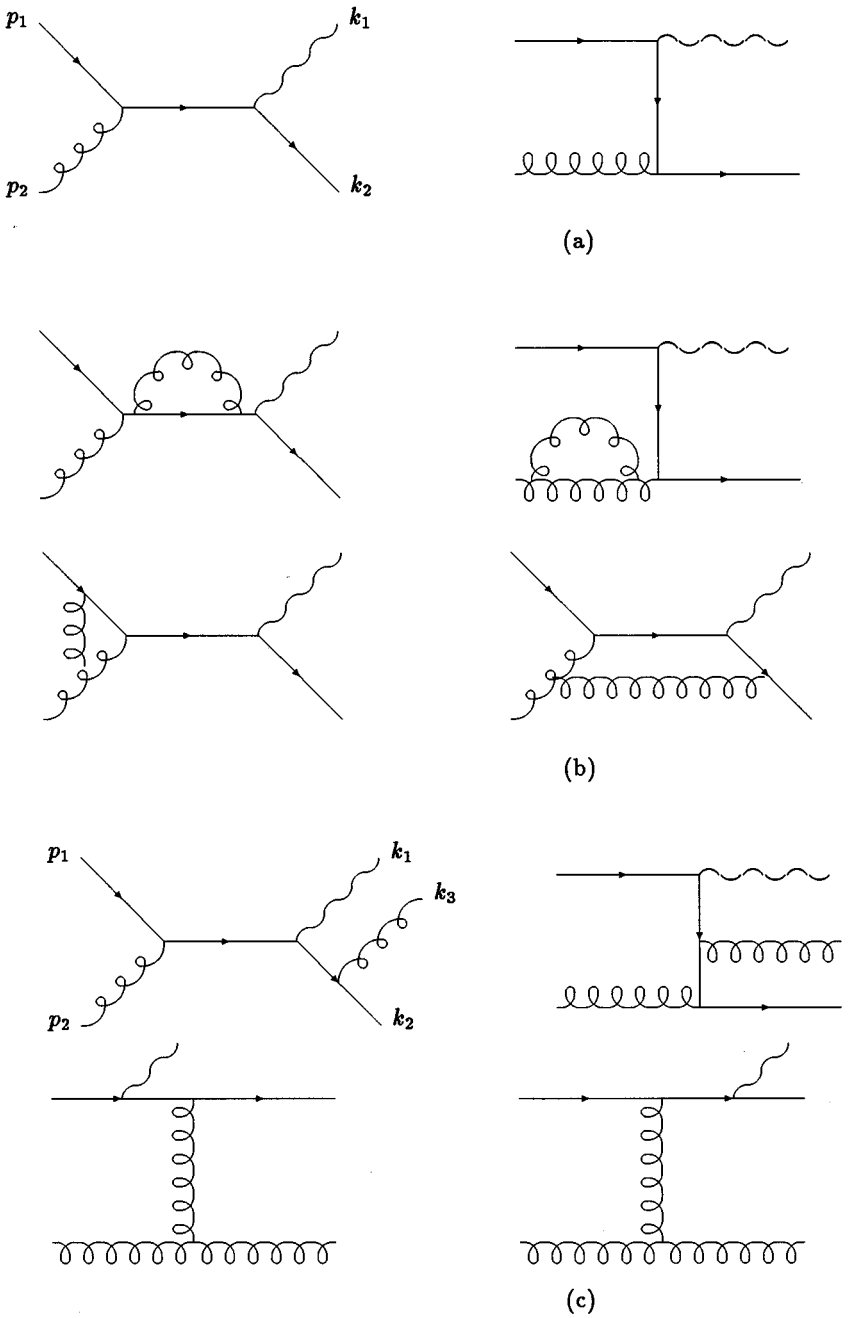

FIG. 1. (a) Lowest order Feynman diagrams for γ plus c quark production; k_1 and k_2 are the four-vector momenta of the photon and charm quark. (b) Examples of virtual corrections to the lowest order diagrams. (c) Examples of next-to-leading order three-body final-state diagrams for the gc initial state.

where $P_{ij}(z)$ are the lowest order splitting functions for parton j into parton i [14] and $\alpha_s(\mu^2)$ is the strong coupling strength.

IV. NUMERICAL RESULTS

In this section we present and discuss several differential cross sections for the joint production of a charm quark and a photon at large values of transverse momentum. All results are displayed for $p\overline{p}$ collisions at the center-of-mass energy $\sqrt{s}=1.8$ TeV appropriate for the Collider Detector at Fermilab (CDF) and D0 experiments at Fermilab. To obtain the differential cross sections presented in this paper, we convolute our hard-scattering matrix elements with the CTEQ3M parton densities [15]. We use the standard two-loop formula for the strong coupling strength with four massless flavors of quarks. We set $\Lambda_{\rm QCD}=0.239$ GeV (the CTEQ3M value). Very similar differential distributions may be obtained if other parton sets are used instead, with quantitative differences reflecting differences among charm quark densities in the different sets [1]. We set the renormalization, factorization, and fragmentation scales to a common value $\mu=p_T^\gamma$ in most of our calculations. Dependence on μ is examined in one of the figures below. Since there are two particles in the final state, the charm quark and the photon, both of whose transverse momenta are large, an alternative choice might be $\mu=p_T^c$ or some function of p_T^γ and p_T^c. The results of our calculations show that the magnitudes of p_T^γ and p_T^c tend to be comparable and that dependence of the cross sections on μ is slight. Therefore, choices of μ different from $\mu=p_T^\gamma$ should not produce significantly different answers, and we

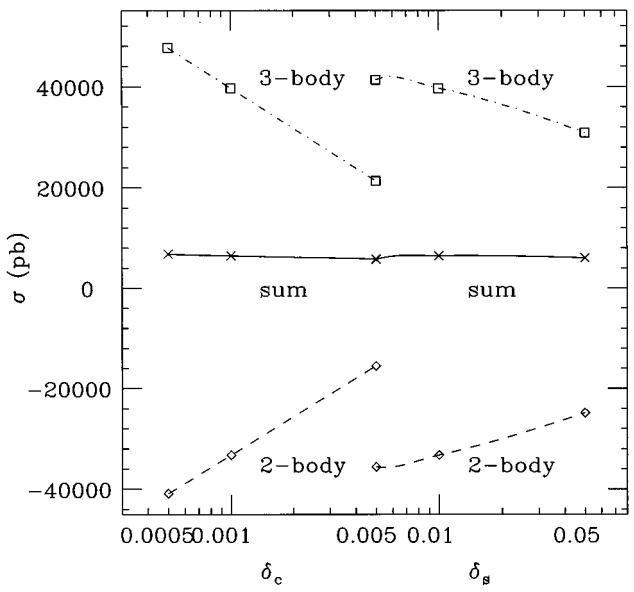

FIG. 2. Study of the dependence of the cross section on the Monte Carlo cutoff parameters δ_s and δ_c. Shown is the cross section for $p+\overline{p}\rightarrow\gamma+c+X$ at $\sqrt{s}=1.8$ TeV with the transverse momenta of the photon and charm quark restricted to the the interval $10<p_T<50$ GeV and the rapidities of the photon and charm quark restricted to the interval $-3.0<y<3.0$.

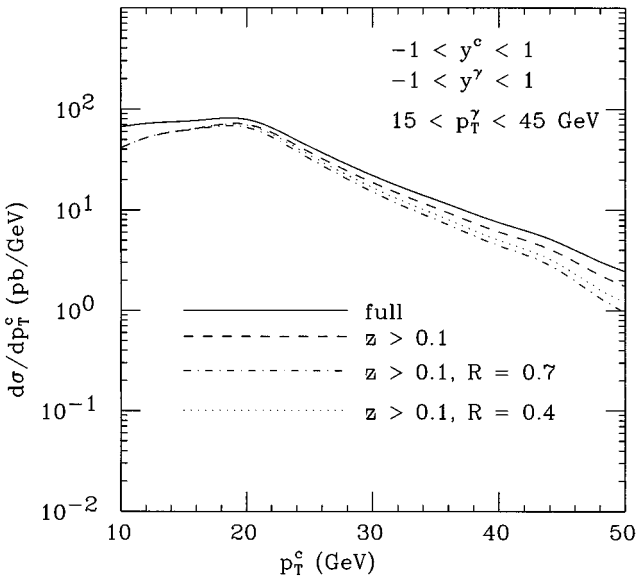

FIG. 3. Cross section $d\sigma/dp_T^c$ as a function of the transverse momentum of the charm quark for $p+\overline{p}\rightarrow\gamma+c+X$ at $\sqrt{s}=1.8$ TeV. The transverse momentum of the photon is restricted to the interval $15<p_T^\gamma<45$ GeV, and the rapidities of the photon and charm quark are restricted to the interval $-1.0<y<1.0$. Four curves are drawn. The solid curve shows the cross section with no further restrictions. The dashed curve indicates the result after the additional selection is made that $z>0.1$; the ratio z is defined in the text. The dotted and dash-dot curves display the results after photon isolation restrictions are applied, in addition to the cut on z.

have verified this supposition in representative cases.

In addition to showing distributions in the rapidities and transverse momenta of the charm quark and the photon, we also discuss distributions in the ratio z, where z is defined as

$$z=-\frac{p_T^c\cdot p_T^\gamma}{(p_T^\gamma)^2}. \tag{4.1}$$

This ratio z is not to be confused with the variable z in the fragmentation functions, Eqs. (3.3) and (3.4). In collider experiments a photon is observed and its momentum is well measured only when the photon is isolated from neighboring hadrons. In our calculation, we impose isolation in terms of the cone variable R:

$$\sqrt{(\Delta y)^2+(\Delta\phi)^2}\leqslant R. \tag{4.2}$$

In Eq. (4.2), Δy ($\Delta\phi$) is the difference between the rapidity (azimuthal angle in the transverse plane) of the photon and that of any parton in the final state. The photon is said to be isolated in a cone of size R if the ratio of the hadronic energy in the cone and the transverse momentum of the photon does not exceed $\epsilon=2$ GeV/p_T^γ. We show distributions for the choices $R=0.7$ and $R=0.4$ typical of current experiments.

Our first figure in this section, Fig. 2, is an examination of the numerical stability of the overall cross section when the cutoff parameters δ_s and δ_c are varied over appropriate ranges. This figure indicates that the combination of analytic and Monte Carlo methods yields consistent numerical results for a broad range of the parameters. For the subsequent figures, we use $\delta_s=0.01$ and $\delta_c=0.001$. We return to a brief examination of the dependence on cutoff parameters when we discuss distributions in the variable z in Fig. 9.

In Fig. 3 we show the differential cross section as a function of the transverse momentum of the charm quark, p_T^c, having restricted the transverse momentum of the photon to the range $15\leqslant p_T^\gamma\leqslant 45$ GeV typical of current hadron collider experiments. The rapidities of the charm quark and photon are restricted to the central region $-1\leqslant y^{\gamma,c}\leqslant 1$ in order to mimic the central region coverage of major collider detectors. The solid curve shows our prediction when no further selections are made other than those mentioned just above. Distributions are presented in the figure for various selections on other kinematic variables. For the dashed curve, the variable z of Eq. (4.1) is restricted to $z\geqslant 0.1$. This selection on z places the photon and charm quark in opposite hemispheres and results in a modest reduction in overall rate. Retaining this cut on z, we examine the effects of isolation of the photon and obtain the results shown by the dotted and dot-dashed curves, for cone sizes of $R=0.4$ and 0.7, respectively.

A common and notable feature of the curves in Fig. 3 is that slopes change near $p_T^c=15$ and 45 GeV. There is a simple reason for this behavior. The contributions to the cross section from two-particle final states produce kinematic configurations in which the photon and charm quark have values of p_T that are equal in magnitude but opposite in sign. Therefore two-body final-state processes cannot contribute in the regions $p_T^c\leqslant 15$ GeV and $p_T^c\geqslant 45$ GeV. Only the three-body final-state processes contribute to the cross section in these regions. The steeper fall of the cross section in either direction away from the region $15\leqslant p_T^c\leqslant 45$ GeV reflects the decreasing likelihood that the photon and charm quark have substantially different values of transverse momentum.

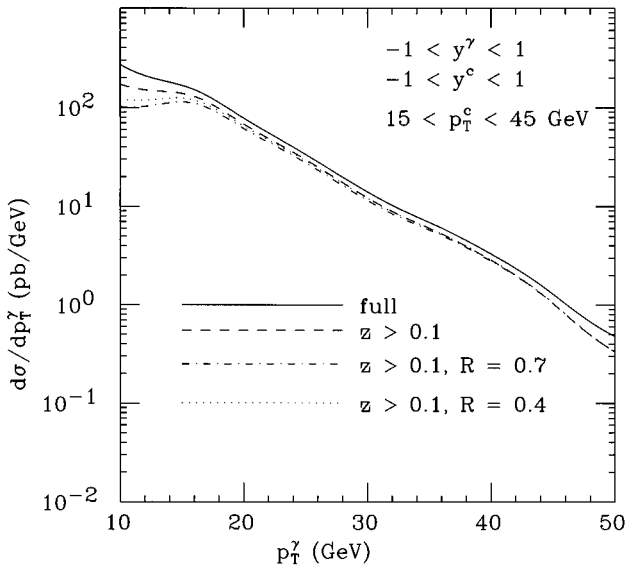

FIG. 4. Cross section $d\sigma/dp_T^\gamma$ as a function of the transverse momentum of the photon for $p+\overline{p}\rightarrow\gamma+c+X$ at $\sqrt{s}=1.8$ TeV. The transverse momentum of the charm quark is restricted to the interval $15<p_T^c<45$ GeV, and the rapidities of the photon and charm quark are restricted to the interval $-1.0<y<1.0$. Four curves are drawn. The solid curve shows the cross section with no further restrictions. The dashed curve indicates the result after the additional selection is made that $z>0.1$; the ratio z is defined in the text. The dotted and dash-dot curves display the results after photon isolation restrictions are applied, in addition to the cut on z.

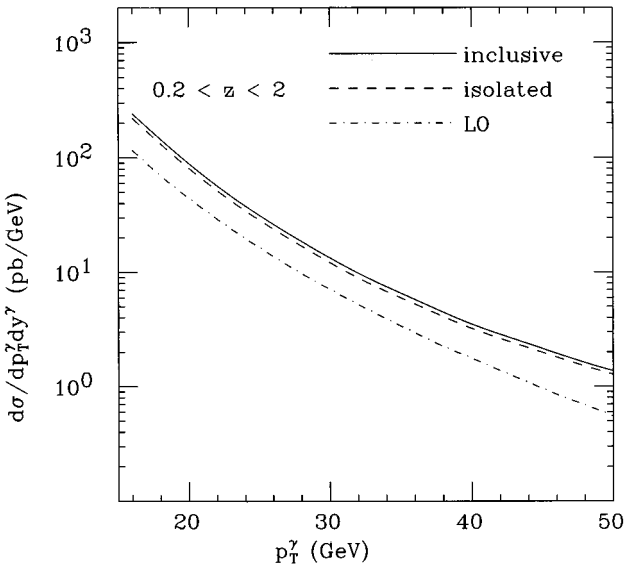

FIG. 5. Cross section $d\sigma/dp_T^\gamma$ as a function of the transverse momentum of the photon for $p+\overline{p}\rightarrow\gamma+c+X$ at $\sqrt{s}=1.8$ TeV. The transverse momentum and rapidity of the charm quark are not restricted, but the rapidity of the photon is limited to the interval $-0.5<y<0.5$. The ratio z is restricted to the interval $0.2<z<2.0$. Three curves are drawn. The solid curve shows the cross section with no further restrictions. The dashed curve indicates the result after photon isolation is imposed, with $R=0.7$, and the dot-dashed curve is the leading-order cross section with photon isolation imposed, $R=0.7$.

Another feature of the results shown in Fig. 3 is that the effect of isolation diminishes as p_T^c is decreased. Isolation affects the cross section principally when the third parton in the final state enters the photon isolation cone and carries transverse momentum greater than the energy resolution threshold. With p_T^γ fixed above 15 GeV, the third parton must be in the charm quark's hemisphere when p_T^c is small in order to balance p_T^γ. When p_T^c is large, the third parton is free to enter the photon isolation cone.

In Fig. 4, we show the cross section differential in p_T^γ. The cuts made are the same as those for Fig. 3, but in this case the charm quark's transverse momentum is restricted between 15 and 45 GeV. The explanation for the change in behavior of the distributions above $p_T^\gamma=45$ GeV and below $p_T^\gamma=15$ GeV is the same as for Fig. 3. An obvious difference between Figs. 3 and 4 is that the effect of photon isolation is most significant in the region of small p_T^γ. The explanation is, again, that with p_T^c restricted above 15 GeV, the third parton in the final state will be found in the photon hemisphere when p_T^γ is small. It is likely to be in the photon isolation cone, and the configuration will be rejected by the isolation cuts.

To examine further the effects of selections on the charm quark momentum, we present in Fig. 5 the cross section differential in the transverse momentum of the photon for a different set of cuts. The photon's rapidity is limited to the range $-0.5\leqslant y^\gamma\leqslant 0.5$, and the ratio z is restricted to $0.2\leqslant z\leqslant 2.0$. These cuts are similar to those of our analytic paper [1]. In Fig. 5, the solid curve represents the cross section with no isolation cuts imposed, and the dashed curve

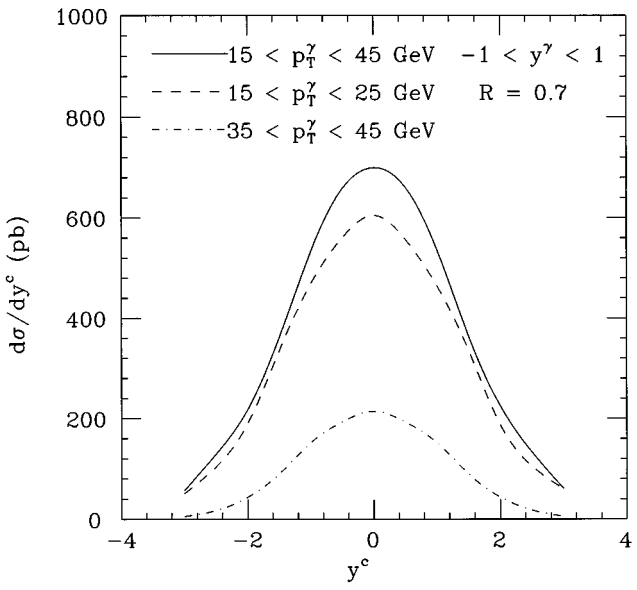

FIG. 6. Cross section $d\sigma/dy^c$ as a function of the rapidity of the charm quark for $p+\overline{p}\rightarrow\gamma+c+X$ at $\sqrt{s}=1.8$ TeV. The photon rapidity is restricted to $-1.0<y^\gamma<1.0$, and photon isolation is imposed, with $R=0.7$. There is no restriction on p_T^c, but the ratio z is restricted to $z>0.1$. Curves are shown for three selections on the transverse momentum of the photon. The solid, dashed, and dot-dashed curves correspond to the selections $15<p_T^\gamma<45$ GeV, $15<p_T^\gamma<25$ GeV, and $35<p_T^\gamma<45$ GeV, respectively. For ease of comparison of shapes, the dot-dashed curve has been multiplied by 10.

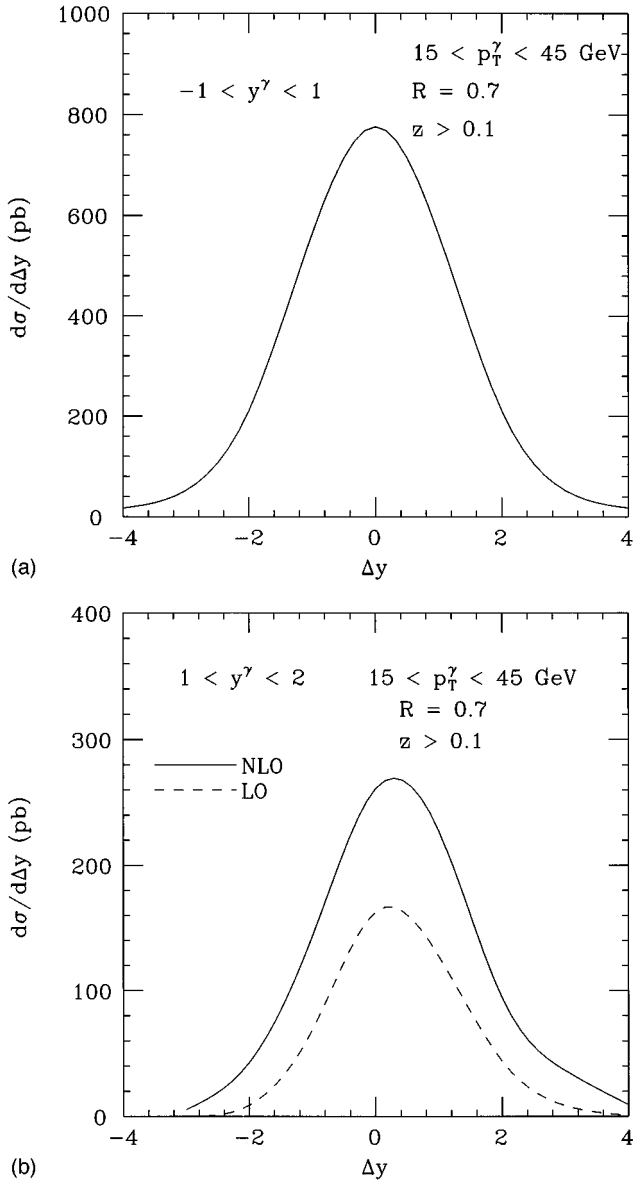

FIG. 7. Cross section $d\sigma/d\Delta y$ as a function of the difference $\Delta y = y^{\gamma} - y^{c}$ of the rapidities of the photon and charm quark, for $p+\overline{p} \to \gamma + c + X$ at $\sqrt{s} = 1.8$ TeV. The ratio z is restricted to $z > 0.1$, and photon isolation is imposed, with $R = 0.7$. The transverse momentum of the photon is selected to be in the interval $15 < p_T^{\gamma} < 45$ GeV. In (a), the photon rapidity is restricted to $-1.0 < y^{\gamma} < 1.0$; in (b) $1.0 < y^{\gamma} < 2.0$. In (b), the dashed curve shows the behavior at leading order.

shows the isolated cross section. The dot-dashed curve is the leading-order prediction, with photon isolation imposed. The behavior seen in Fig. 5 is clearly different from that of Fig. 4 in that the cross section does not fall off in the region of small p_T^{γ}, as expected, since there in no selection in Fig. 5 on p_T^{c} (other than the selection on z).

In Fig. 6 we show the distribution in the rapidity of the charm quark, y^{c}, for different cuts on the photon's transverse momentum. In all cases $-1 \leqslant y^{\gamma} \leqslant 1$. The distribution in y^{c} is fairly broad, with a full width at half maximum of about 3.2 units in rapidity. The dashed and dot-dashed curves show that the distribution in y^{c} may broaden somewhat as p_T^{γ} is increased.

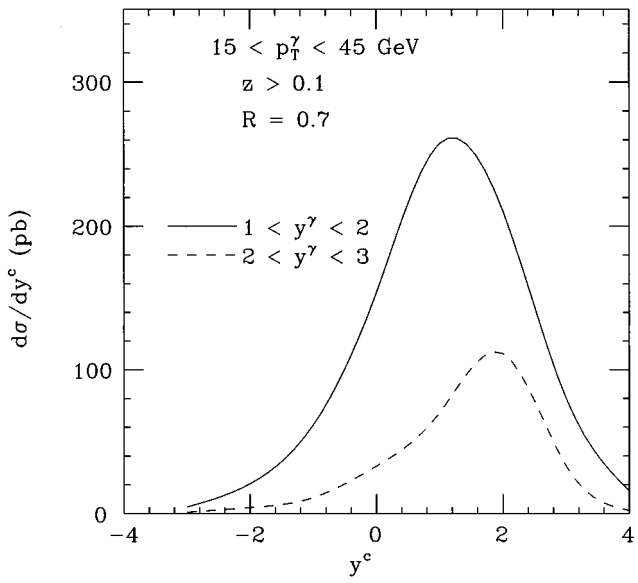

FIG. 8. Cross section $d\sigma/dy^{c}$ as a function of the rapidity of the charm quark for $p+\overline{p} \to \gamma + c + X$ at $\sqrt{s} = 1.8$ TeV. Photon isolation is imposed, with $R = 0.7$, $z > 0.1$, and $15 < p_T^{\gamma} < 45$ GeV. The solid curve shows the result when the photon rapidity is restricted to $1.0 < y^{\gamma} < 2.0$, and the dashed curve displays the result for $2.0 < y^{\gamma} < 3.0$.

The structure of the QCD hard-scattering matrix element produces *positive* correlations in rapidity [16] at collider energies. To examine correlations more precisely, we study the cross section as a function of the difference of the rapidities of the photon and charm quark. Results are shown in Fig. 7. In Fig. 7(a), we see that the distribution in Δy is narrower than the corresponding distribution in y^{c} shown in Fig. 6. The broader distribution in Fig. 6 results from a spread of the approximately Gaussian and relatively narrow dynamical distribution of Fig. 7(a) over the range $-1 \leqslant y^{\gamma} \leqslant 1$. In Fig. 7(b), we select photons whose rapidities are in the forward hemisphere, $1.0 < y^{\gamma} < 2.0$. We observe that the peak in the Δy distribution remains close to $\Delta y = 0$, reflecting the predicted [16] positive dynamical correlations, but with the typical value of y^{c} lagging somewhat behind that of the selected y^{γ}.

In Fig. 8, we display the differential cross section in y^{c} itself, for two intervals of y^{γ} in the forward rapidity region. These distributions show how the typical rapidity of the charm quark follows that of the photon.

The dependence of the cross section on the variable z, defined in Eq. (4.1), is indicative of the imbalance in transverse momentum of the charm quark and the photon. For two-body processes, such as the leading-order Compton subprocess $gc \to \gamma c$, the photon and charm quark have balancing transverse momenta, and the distribution is a δ function in z, $\delta(1-z)$. Contributions away from $z = 1$ are due to the higher order three-body contributions or to fragmentation processes. As discussed in Ref. [1], the photon fragmentation processes contribute in the region $z \geqslant 1$ only. Processes in which the charm quark is produced via fragmentation contribute in the region $0 \leqslant z \leqslant 1$. We thus expect that the effect of photon isolation will be observed in the region $z \geqslant 1$. This expectation is confirmed in the results of Fig. 9(a) that show

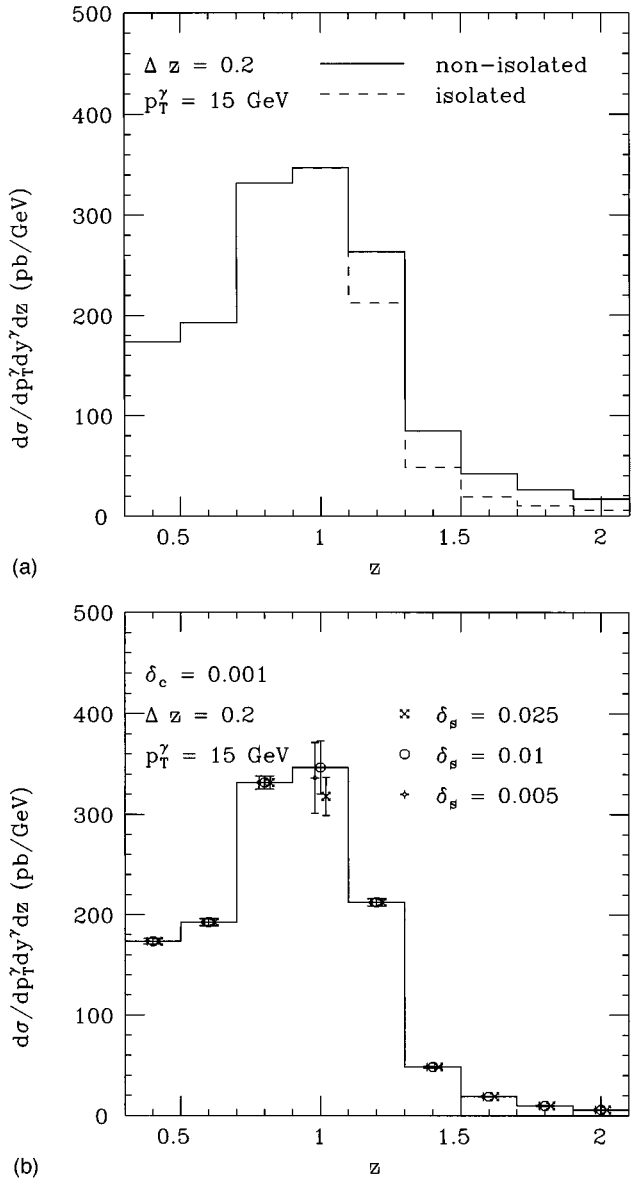

FIG. 9. Cross section $d\sigma/dp_T^\gamma dy^\gamma dz$ as a function of the ratio z for $p+\overline{p}\rightarrow\gamma+c+X$ at $\sqrt{s}=1.8$ TeV. The transverse momentum and rapidity of the photon are averaged over the intervals $14<p_T^\gamma<16$ GeV and $-0.5<y^\gamma<0.5$. In (a), we illustrate the effects of photon isolation by comparing the distributions in z with and without the isolation restriction. The solid histograms in (b) and (c) show the results of our calculation for our standard Monte Carlo integration cutoff parameters $\delta_s=0.01$ and $\delta_c=0.001$. In (b) and (c), photon isolation is imposed with $R=0.7$. In (b), we display the dependence of the final cross section on the Monte Carlo integration cutoff parameter δ_s, having fixed $\delta_c=0.001$. In (c), we show the dependence of the final cross section on the cutoff parameter δ_c, having fixed $\delta_s=0.01$.

the cross section as a function of z for the nonisolated and isolated cases. The solid histogram in Fig. 9(a) agrees quantitatively with the corresponding histogram in our analytic paper [1] except for differences associated with the different choice of parton densities.

The δ-function behavior at leading order is, of course, moderated by nonperturbative effects associated with the ''intrinsic'' transverse momentum of the initial partons as well as by next-to-leading order perturbative contributions. In this paper, we are working in the usual purely perturbative framework in which the initial partons are assumed to be collinear. For a three-parton final state, the region of z near unity is the region in which one of the three final partons becomes soft. Sensitivity to soft-gluon effects and the necessity for resummation procedures is a common limitation when one considers next-to-leading order contributions to an observable that is proportional to a δ function in leading order. In our calculation the soft-gluon corrections to the three-body processes are considered as effective two-body contributions, as discussed in Sec. II. These contribute to the cross section at $z=1$, meaning that all dependence on the soft cutoff parameter δ_s is concentrated at $z=1$. In Fig. 9(b) we show the distribution in z for different values of δ_s. The cross section is fairly independent of this parameter except when it becomes larger than about 0.02. Similarly, in Fig. 9(c), we examine dependence on δ_c, the collinear cutoff parameter. We find fair stability over a reasonable range of values of δ_c. The observed δ_c variation is similar to the scale dependence seen in Fig. 6 of Ref. [1]. The two have a related physical origin. In the approach of Ref. [1], the choice of a scale μ partitions the calculation arbitrarily into two-body collinear and three-body final-state contributions. If μ is increased, more of the next-to-leading order QCD contributions are placed into the parton distributions (collinear kinematics) and less into the exact three-body kinematics. Likewise, here the parameter δ_c partitions the overall QCD matrix element into two-body collinear and three-body final-state contributions. It therefore is not a surprise to see the same type of variation with δ_c in Fig. 9(c) as is exhibited by scale variation.

The infrared sensitivity of the distribution in z, reflected in the δ_s dependence discussed above and in the scale de-

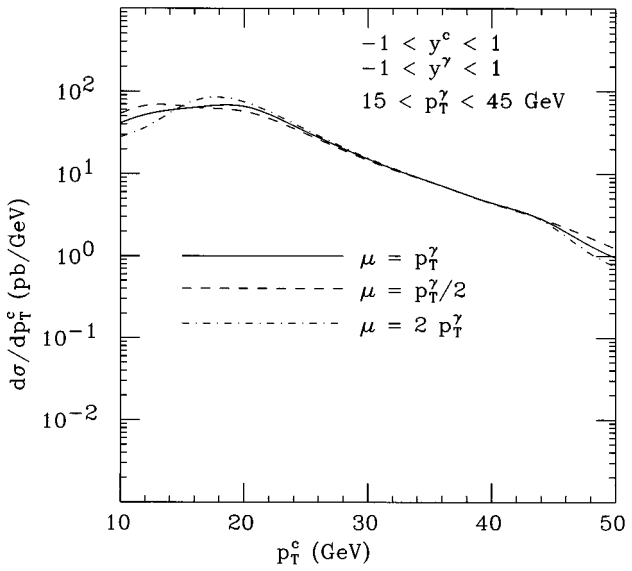

FIG. 10. The renormalization or factorization scale (μ) dependence of the cross section is displayed. Shown is the transverse momentum dependence of $d\sigma/dp_T^c$ for three values of μ/p_T^γ: 0.5, 1.0, and 2. The transverse momentum of the photon is restricted to the interval $15<p_T^\gamma<45$ GeV, and the rapidities of the photon and charm quark are restricted to the interval $-1.0<y<1.0$.

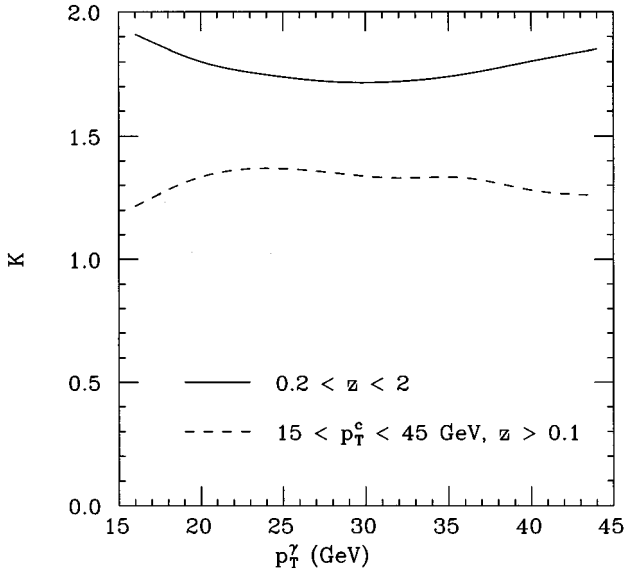

FIG. 11. The K factor defined in the text is shown as a function of p_T^γ. Photons are isolated with $R = 0.7$. The solid line corresponds to selections analogous to those of our analytic paper [1], $-0.5<y^\gamma<0.5$ and $0.2<z<2.0$, but with no restrictions on y^c or p_T^c. The dashed line shows how results change when the transverse momentum of the charm quark is restricted to the interval $15<p_T^c<45$ GeV with, in addition, $z>0.1$ and the rapidities of the photon and charm quark limited to the interval $-1.0<y<1.0$.

pendence examined in Ref. [1], means that the z distribution at may not be calculated sufficiently reliably at next-to-leading order. Resummation of the effects of soft-gluon radiation is required, particularly in the region near $z=1$.

The renormalization, factorization, or fragmentation scale dependence of our isolated cross section is illustrated in Fig. 10 as a function of p_T^c. The cuts are those of Fig. 3 for cone size $R=0.7$. All three scales are varied simultaneously, $\mu=np_T^\gamma$. The dependence on scale is negligible in the region $15\leqslant p_T^c\leqslant 45$ GeV, whereas outside this region we see some dependence. As remarked earlier in our discussion of Fig. 3, both two-body and three-body processes contribute to the cross section in the region $15\leqslant p_T^c\leqslant 45$. In this region, the next-to-leading order process is complete in the sense that there are both $O(\alpha_s)$ and $O(\alpha_s^2)$ contributions. The factorization scales in the hard subprocess cross section compensate and cancel those in the structure and fragmentation functions. In the regions $p_T^c\leqslant 15$ GeV and $p_T^c\geqslant 45$ GeV, only three-body processes contribute. There are no factorization scales in the hard subprocess cross sections, except for photon fragmentation scales in the latter region, to compensate the scale dependence of the structure functions. The absence of compensating terms results in the observed scale dependence in these regions, particularly in the region of small p_T.

A useful measure of the importance of next-to-leading order contributions is the ''K factor,'' defined as the ratio of the full cross section through next-to-leading order to the full leading-order cross section, with fragmentation included. We provide values of K in Fig. 11 as a function of p_T^γ for two different sets of kinematic selections. Both curves represent isolated photon cross sections with $R=0.7$. The solid curve is the K factor appropriate to the selections of our Fig. 5. A value of K near 1.5 is in agreement with preliminary experimental indications [2]. The dashed curve in Fig. 11 is the K factor for the cross section with the cuts specified in Fig. 4.

V. SUMMARY AND DISCUSSION

In this paper we present the results of a calculation of the inclusive production of a prompt photon in association with a heavy quark at large values of transverse momentum. This analysis is done at next-to-leading order in perturbative QCD. We employ a combination of analytic and Monte Carlo integration methods in which infrared and collinear singularities of the next-to-leading order matrix elements are handled properly. Our results agree quantitatively with those we obtained using purely analytic methods [1], as they should, but the combination of analytic and Monte Carlo methods used in this paper is more versatile. We provide differential cross sections in transverse momenta and rapidity, including photon isolation restrictions, that should facilitate contact with experimental results at hadron collider energies. We show that the study of two-particle inclusive distributions, with specification of the momentum variables of both the final prompt photon and the final heavy quark, tests correlations inherent in the QCD matrix elements [16] and should provide a means for measuring the charm quark density in the nucleon [1]. Our results are presented in terms of the transverse momentum of the charm quark. In a typical experiment [2], the momentum of the quark may be inferred from the momentum of prompt lepton decay products or the momentum of charm mesons, such as D^*'s. Alternatively, our distributions in p_T^c may be convoluted with charm quark

fragmentation functions, deduced from, e.g., e^+e^- annihilation data, to provide distributions for the prompt leptons or D^*'s.

ACKNOWLEDGMENTS

The work at Argonne National Laboratory was supported by the U.S. Department of Energy, Division of High Energy Physics, Contract No. W-31-109-ENG-38. This work was supported in part by Eckerd College.

APPENDIX: ANALYTIC EXPRESSIONS

In order to make this paper reasonably self-contained, we collect in this appendix all the formulas we use in the calculation. If we label the momenta for the generic three-body final-state process by

$$p_1+p_2\rightarrow p_3+p_4+p_5, \tag{A1}$$

where p_3 denotes the photon and p_4 denotes the observed charm quark, we can define the Mandelstam invariants

$$\hat{t}=(p_1-p_3)^2,$$

$$\hat{u}=(p_2-p_3)^2,$$

$$\hat{s}=(p_1+p_2)^2. \tag{A2}$$

We express the two-body final-state cross sections in terms of the scaled variable v, where

$$v=1+\frac{\hat{t}}{\hat{s}}. \tag{A3}$$

1. Two-body contributions

The effective two-body contribution includes the $O(\alpha_s^2)$ virtual gluon-exchange loop contributions and the soft and/or collinear parts of the three-body contributions (this remark applies to initial-state collinear contributions only, as explained later). After all soft pole singularities are canceled and all collinear pole singularities are factored, the effective two-body contribution is expressed as

$$\sigma_{2\,\mathrm{body}}(A+B\rightarrow\gamma+c+X)=\int dv\,dx_1\,dx_2 \times\left[\frac{d\sigma_{\mathrm{coll}}^{cg\rightarrow\gamma c}}{dv}+f_g^A(x_1,M^2) \times f_c^B(x_2,M^2)\frac{d\sigma^{\mathrm{HO}}}{dv}(cg\rightarrow\gamma c)\right], \tag{A4}$$

plus terms in which the beam and target are interchanged. In this section we use the subscript c to refer to the charm quark (or antiquark).

We define

$$T_{cg}=\frac{2-2v+v^2}{1-v}, \tag{A5}$$

and $v_1=1-v$. In Eq. (A4),

$$\begin{aligned}\frac{d\sigma^{\mathrm{HO}}}{dv}(cg\rightarrow\gamma c)=\frac{\pi\alpha_{\mathrm{em}}\alpha_s e_c^2}{\hat{s}N_C}\Bigg\{ & T_{cg}+\frac{\alpha_s}{2\pi}\Bigg[\frac{1}{2}\Bigg(\frac{N_F}{3}T_{cg}-14C_FT_{cg}+2N_C\ln v_1+4(2C_F+N_C)T_{cg}\ln^2\delta_s-\frac{2}{3}N_FT_{cg}\ln\frac{\hat{s}}{M^2} \\ & +C_FT_{cg}(3+4\ln\delta_s)\ln\frac{\hat{s}}{M^2}+C_FT_{cg}(3+4\ln\delta_s)\ln\frac{\hat{s}}{M''^2}+\frac{1}{3}N_CT_{cg}(11+12\ln\delta_s)\ln\frac{\hat{s}}{M^2} \\ & +\frac{1}{3}(11N_C-2N_F)T_{cg}\ln\frac{\hat{s}}{\mu^2}+4(2C_F-N_C)\ln v+4T_{cg}\ln\delta_s(N_C\ln v_1+2C_F\ln v-N_C\ln v) \\ & +N_C(1+v)\ln^2 v_1+(2C_F-N_C)\frac{(2-2v+3v^2)}{v_1}\ln^2 v+2C_F\frac{(1+2v)}{v_1}\ln v_1-N_C\pi^2\frac{(-1-2v+4v^2)}{3v_1} \\ & +2C_F\pi^2\frac{(1-4v+5v^2)}{3v_1}+2C_F\frac{(v^2+v_1^2)}{v_1}\ln^2 v_1-2(2C_F-N_C)\frac{(v^2+v_1^2)}{v_1}\ln v\ln v_1 \\ & +2(2C_F-N_C)T_{cg}\mathrm{Li}_2(1-v)+2N_CT_{cg}\mathrm{Li}_2(v)\Bigg)\Bigg]\Bigg\}.\end{aligned} \tag{A6}$$

The scales M and M'' are the factorization and fragmentation scales, respectively, on the initial parton and final-state charm quark legs, and μ is the renormalization scale. $C_F=4/3$ is the quark-gluon vertex color factor, $N_C=3$ is the number of colors, e_c is the fractional charge of the charm quark, δ_s and δ_c are the soft and collinear cutoff parameters defined in Sec. II, $\mathrm{Li}_2(x)$ is the dilogarithm function, and α_{em} is the electromagnetic coupling constant.

The remnants of the factorization of the hard collinear singularities are

$$\frac{d\sigma_{\rm coll}^{cg\to\gamma c}}{dv}=\frac{\alpha_{\rm em}\alpha_s^2 e_c^2}{2\hat{s}}\frac{1}{N_C}T_{cg}\left[f_g^A(x_1,M^2)\left(\int_{x_2}^{1-\delta_s}\frac{dz}{z}f_c^B\left(\frac{x_2}{z},M^2\right)\widetilde{P}_{qq}(z)+\int_{x_2}^{1}\frac{dz}{z}f_g^B\left(\frac{x_2}{z},M^2\right)\widetilde{P}_{qg}(z)\right)+f_c^B(x_2,M^2)\right.$$
$$\left.\times\left(\int_{x_1}^{1-\delta_s}\frac{dz}{z}f_g^A\left(\frac{x_1}{z},M^2\right)\widetilde{P}_{gg}(z)+\int_{x_1}^{1}\frac{dz}{z}f_q^A\left(\frac{x_1}{z},M^2\right)\widetilde{P}_{gq}(z)\right)\right]. \tag{A7}$$

The last distribution $f_q^A(x_1,M^2)$ in Eq. (A7) implies a sum over the flavors of quarks from the $c\bar{c}$, cq, and $c\bar{q}$ initial states. The remaining two processes $c\bar{c}$ and $q\bar{q}$ do not have initial-state collinear singularities and thus do not contribute to this part of the cross section. Equation (A7) differs slightly from that given in Ref. [8], where the upper limit of integration was always taken to be $1-\delta_s$. In principle, this is incorrect since it implies that processes other than the cg-initiated process may have soft singularities, but the error introduced by that approximation is very small for small δ_s. We use the correct expression in our calculation.

The splitting functions $\widetilde{P}_{ij}$, listed in the Appendix of Ref. [8], are included here for completeness:

$$\widetilde{P}_{ij}(z)=P_{ij}(z)\ln\left(\frac{1-z}{z}\delta_c\frac{\hat{s}}{M^2}\right)-P'_{ij}(z). \tag{A8}$$

The functions $P_{ij}(z)$ are the usual Altarelli-Parisi splitting functions in $4-2\epsilon$ dimensions and are

$$P_{qq}(z,\epsilon)=C_F\left[\frac{1+z^2}{1-z}-\epsilon(1-z)\right], \tag{A9}$$

$$P_{qg}(z,\epsilon)=\frac{1}{2(1-\epsilon)}[z^2+(1-z)^2-\epsilon],$$

$$P_{gg}(z,\epsilon)=2N_C\left[\frac{z}{1-z}+\frac{1-z}{z}+z(1-z)\right],$$

$$P_{gq}(z,\epsilon)=C_F\left[\frac{1+(1-z)^2}{z}-\epsilon z\right].$$

The functions $P'_{ij}(z)$ are defined by the relation

$$\widetilde{P}_{ij}(z,\epsilon)=P_{ij}(z)+\epsilon P'_{ij}(z). \tag{A10}$$

2. Pseudo-two-body contributions

Since we are interested in distributions in the kinematic variables of two final-state partons, the photon and the c quark, we can define variables that depend on the momenta of both. An example is the variable z, defined in Eq. (4.1). Whenever there is a third parton in the final state, the distribution in z (or in other analogous variables) will differ from a δ function when the third parton carries a finite momentum, even if it is collinear to one of the other final partons. For this reason we designate as ''pseudo-two-body contributions'' those for which the third parton is collinear to either the final photon or the charm quark. These contributions are expressed, respectively, by the equations

$$\sigma_{\gamma/\rm coll}=\sum_{abcq}\int f_a^A(x_1,M^2)f_b^B(x_2,M^2)\left(\frac{\alpha_{\rm em}}{2\pi}\right)\left[P_{\gamma q}(z)\ln\left[z(1-z)\delta_c\frac{\hat{s}}{M'^2}\right]-P'_{\gamma/q}(z)\right]\frac{d\hat{\sigma}}{dv}(ab\to cq)dx_1dx_2dzdv \tag{A11}$$

and

$$\sigma_{c/\rm coll}=\sum_{abd}\int f_a^A(x_1,M^2)f_b^B(x_2,M^2)\widetilde{P}_{cd}(z,M''^2)\frac{d\hat{\sigma}}{dv}(ab\to\gamma d)dx_1dx_2dzdv. \tag{A12}$$

The functions $P_{\gamma/q}(z)$ and $P'_{\gamma/q}(z)$ are the quark-to-photon splitting function and $O(\epsilon)$ piece, respectively. They have the same form as P_{gq}, with the color factor replaced by the square of the quark charge. The scale M' is the fragmentation scale for quark fragmentation into a photon.

$$\widetilde{P}_{cd}(z,M''^2)=P_{cd}(z)\ln\left[z(1-z)\delta_c\frac{s}{M''^2}\right]-P'_{cd}(z), \tag{A13}$$

where $P_{cd}(z)$ represents the splitting functions $P_{qg}(z)$ and $P_{qq}(z)$ of Eq. (A9) along with the ''primed'' pieces. In Eq. (A11), q can be a charm quark or charm antiquark or a (anti)quark of any flavor in the case of $cq\to cq$. In Eq. (A12), d is either a gluon or charm quark or charm antiquark.

These contributions are usually referred to as the remnants of the factorization of the hard collinear singularities and are regarded as two-body processes or as parts of the fragmentation contributions because of their dependence on the factorization scales. We prefer to regard them as pseudo-two-body contributions. When we examine either the charm quark or photon momentum distributions, these contributions populate the same regions of phase space as the other three-body contributions in Eq. (A17), unlike the effective two-

body contributions. The pseudo-two-body contributions are usually negative in overall sign due to the large logarithms of the cutoff parameters, as are the two-body contributions discussed above.

3. Photon fragmentation contributions

As mentioned in Sec. III, we include the quark-to-photon and gluon-to-photon fragmentation contributions at leading order only. We convolute the $2\to2$ hard-scattering subprocess cross sections for the processes listed in Eq. (3.1) with photon fragmentation functions $D_{\gamma/i}(z,M'^2)$; M' is the fragmentation scale, the same scale at which we subtract the collinear singularities on the photon leg of the three-body processes. The expression for the cross section is

$$\sigma_{\mathrm{frag}/\gamma}=\sum_{abj}\int f_a^A(x_1,M^2)f_b^B(x_2,M^2)D_{\gamma/j}(z,M'^2)\times\frac{d\hat{\sigma}}{dv}(ab\to jc)dx_1dx_2dzdv. \tag{A14}$$

The matrix elements for the hard subprocess cross section are well known and can be found, for example, in Ref. [4].

4. Charm fragmentation contributions

In integrating some of the three-body matrix elements over phase space we encounter configurations in which the charm quark is produced collinearly with a charm antiquark or a gluon in the final state. These situations lead to a collinear singularity in the massless approximation. They occur for the processes of Eq. (2.1a), (2.1c), and (2.1f). We factor these singularities into a fragmentation function $D_{c/i}(z,M''^2)$ for parton i to produce a charm quark with momentum fraction z. The contributing subprocess cross sections are

$$\frac{d\hat{\sigma}}{dv}(q\bar{q}\to\gamma g)=\frac{2C_F}{N_C}\frac{\pi\alpha\alpha_s e_q^2}{s}\left(\frac{v}{1-v}+\frac{1-v}{v}\right),$$

$$\frac{d\hat{\sigma}}{dv}(qg\to\gamma q)=\frac{\pi\alpha\alpha_s e_q^2}{N_C s}\left(\frac{1+(1-v)^2}{1-v}\right). \tag{A15}$$

The physical cross section is given by

$$\sigma_{\mathrm{frag}/c}=\sum_{abd}\int f_a^A(x_1,M^2)f_b^B(x_2,M^2)D_{c/d}(z,M''^2)\times\frac{d\hat{\sigma}}{dv}(ab\to\gamma d)dx_1dx_2dzdv. \tag{A16}$$

5. Three-body contributions

The noncollinear three-body final-state contributions are calculated from the expression

$$\sigma_{3\mathrm{body}}=\sum_{abd}\int f_a^A(x_1,M^2)f_b^B(x_2,M^2)\times d\hat{\sigma}(ab\to\gamma cd)dx_1dx_2d\Omega, \tag{A17}$$

with Ω representing the angles and other variables that are integrated over. Whenever an invariant s_{ij} or t_{ij} falls into a collinear or soft region of phase space, that contribution from the subprocess is excluded. The three-body contribution shows no dependence on the factorization scale of the final-state charm or photon legs, although we have factored collinear singularities at scales M'' and M', respectively, on these legs of the three-body subprocesses. However, Eq. (A17) does contain an implicit logarithmic dependence on the soft and, in particular, the collinear cutoffs discussed in Sec. II. Both collinear cutoff and factorization scale dependences are contained in the pseudo-two-body contributions discussed above.

[1] E. L. Berger and L. E. Gordon, this issue, Phys. Rev. D **54** 2279 (1996), and references therein.

[2] CDF Collaboration, R. Blair *et al.*, in *Proton-Antiproton Collider Physics*, edited by R. Raja and J. Yoh, AIP Conf. Proc. No. 357 (AIP, New York, 1996), pp. 557–567.

[3] E. L. Berger, E. Braaten, and R. D. Field, Nucl. Phys. **B239**, 52 (1984).

[4] D. W. Duke and J. F. Owens, Phys. Rev. D **26**, 1600 (1982); J. F. Owens, Rev. Mod. Phys. **59**, 465 (1987).

[5] P. Aurenche *et al.*, Nucl. Phys. **B399**, 34 (1993).

[6] M. Glück, E. Reya, and A. Vogt, Phys. Rev. D **48**, 116 (1993).

[7] E. L. Berger and J.-W. Qiu, Phys. Lett. B **248**, 371 (1990); Phys. Rev. D **44**, 2002 (1991); E. L. Berger, X. Guo, and J.-W. Qiu, Phys. Rev. Lett. **76**, 2234 (1996).

[8] H. Baer, J. Ohnemus, and J. F. Owens, Phys. Rev. D **42**, 61 (1990).

[9] B. Bailey, J. Ohnemus, and J. F. Owens, Phys. Rev. D **46**, 2018 (1992).

[10] H. Baer and H. Reno, Phys. Rev. D **43**, 2892 (1991).

[11] J. Ohnemus and J. F. Owens, Phys. Rev. D **43**, 3626 (1991); J. Ohnemus, *ibid.*, **44**, 1403 (1991); **44**, 3477 (1991).

[12] M. Stratmann and W. Vogelsang, Phys. Rev. D **52**, 1535 (1995).

[13] L. E. Gordon and W. Vogelsang, Phys. Rev. D **48**, 3136 (1993); **50**, 1901 (1994); M. Glück, L. E. Gordon, E. Reya, and W. Vogelsang, Phys. Rev. Lett. **73**, 388 (1994).

[14] G. Altarelli and G. Parisi, Nucl. Phys. **B126**, 298 (1977).

[15] H. L. Lai *et al.*, Phys. Rev. D **51**, 4763 (1995).

[16] E. L. Berger, Phys. Rev. D **37**, 1810 (1988).